COBEM 2021 26th International Congress of Mechanical Engineering
November 22-26, 2021, Virtual Congress, Brazil

COB-2021-0535
CFD ANALYSIS OF A MORPHING WING FOR AERONAUTIC APPLICATIONS

Nicolas Guimarães Ono
Lucas Funari Antunes
Giovanna Scala
Caio Elias Ribeiro
Bruno Galelli Chieregatti, PhD
Instituto Mauá de Tecnologia, Praça Mauá, 1, São Caetano do Sul, SP, Brasil
nic.ono@hotmail.com

Abstract. *Changing the camber in an airfoil is an effective way to increase the lift generated and potentially improve the aerodynamic efficiency. It can be achieved either by using conventional trailing edge flaps or using the morphing wing concept, which create smooth and continuous changes in the geometry instead of the sudden change caused by the plain flaps mechanism that leads to performance drawbacks and sub-optimal fly conditions. Recently a new category of Morphing Wing was developed by researchers at the Swansea University, named Fishbone Active Camber (FishBAC). This article aims to analyze and compare the aerodynamic performance of airfoils that uses plain flaps with airfoils that use the FishBAC concept. The airfoils chosen are the low Reynolds number symmetric Eppler 472 and the asymmetric Eppler 374. Two different methods were used, a panel method code, XFOIL, applied in the XFLR5 software, and the ANSYS-FLUENT, a different finite volume solver and high-fidelity Computational Fluid Dynamics (CFD) software. The studies showed a significant improvement in lift-to-drag ratios along the angles of attack for the configurations using morphing concept due to the low drag penalty when compared to the same lift coefficient value for flapped airfoils.*

Keywords: *Morphing Wing, camber, airfoil, Computational Fluid Dynamics (CFD), FishBAC*

1. INTRODUCTION

The human desire to fly has always been fueled by the observation of flight in nature, motivating the continuous development of aircraft that nowadays are so commonly used. Though, flying was not the only inspiration, designer's approach until today is to achieve the simplicity, elegance and efficiency that animals obtained by thousand years of biological evolution. Mostly, the wings movement and adaptability when facing different situations requiring abrupt changes in its shape. (Barbarino, Bilgen, Ajaj, Friswell, & Inman, 2011)

The introduction of discrete trailing edge control surfaces as conventional flaps, ailerons or slats in commercial aircrafts enabled the geometry and shape change. However, the discrete camber variation is not a smooth transition of camber in the chord-wise direction. It leads to a similarly abrupt change in the pressure distribution over the corner created at the hinge line causing drag penalty outcome and risk of boundary layer separation. Nowadays the focus is to minimize abrupt changes in the pressure distribution and avoid as much boundary layer separation. These two phenomena are the main cause of drag, which increases fuel consumption therefore it must not be left aside.

Recently a new technology is beginning to be introduced in small planes and drones, in which a smooth but effective change in the camber of the airfoil profile provides the best performance thru a range of flying conditions. This technology is called Morphing Wing, as the profile can have either slight or major changes in its camber, without creating discontinuity. This concept reduces the drag and keeps the lift to drag coefficient in good levels, leading to fuel economy. Historically, morphing studies have shown penalties in terms of complexity, weight and cost. However, in some cases the aerodynamic benefits overcome these circumstances, especially with the current trend for efficient and sustainable aircraft rewrites the priorities, as the development of new materials and the novelties of the manufacturing methods.

A study directed by NASA shows that a 1% reduction in drag coefficient on a commercial airline plane can save up to 140 million dollars in the US airline fleet, when considering a cost of 70 cents per gallon of fuel. For a middle range aircraft using the morphing concept, the reduction that is seen varies between 3% and 5%, depending on the distance and flight mission. It can show how the change on the camber variation would impact on the airplane performance and cost. (Barbarino, Bilgen, Ajaj, Friswell, & Inman, 2011)

In this context, recently a new category of Morphing Wing was developed by researchers at the Swansea University, named Fishbone Active Camber (FishBAC). It is a biologically inspired compliant structure of a thin chordwise bending beam spine with stringers branching off to connect it to a pre-tensioned Elastomeric Matrix Composite (EMC) skin surface

which motivated by a design that had already being employed by NASA in the past. The Figure 1 shows the prototype with Morphing concept made by Swansea researchers applied to turbulent flow (Re = 3 x 10^6). (Woods & Friswell, 2012)

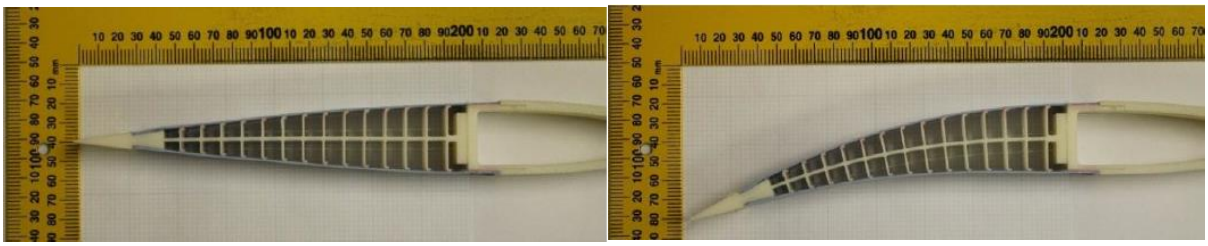

Figure 1. Morphing Wing FishBAC prototype unmorphed (left) and deflected (right).
(Woods & Friswell, 2012)

Therefore, the present work consists of an expansion of the study of the FishBAC Morphing concept with a $3 \times 10^5 \leq Re \leq 5 \times 10^5$, via XFOIL panel method and CFD analysis, to compare the aerodynamic advantage of the morphing wing versus a flap system. In fact, verifying the best aerodynamic efficiency of this technological innovation, and shows the ability to generate improvements on the aircraft design, thus enhance its performance and reducing fuel consumption, which, consequently, reduces operating costs and minimizes the emission of polluting gases, contributing to the environment.

2. METHODOLOGY

2.1 Airfoil Geometry Definition

In the present work both low Reynolds airfoils, Eppler 472 and Eppler 374, were used to create camber morphing airfoil geometries representative of the FishBAC concept. The first is a symmetric profile, has a maximum thickness of 12% at 17.5% chord. The second is asymmetric profile that has a maximum thickness of 10.9% at 34.3% chord and camber of 2%.

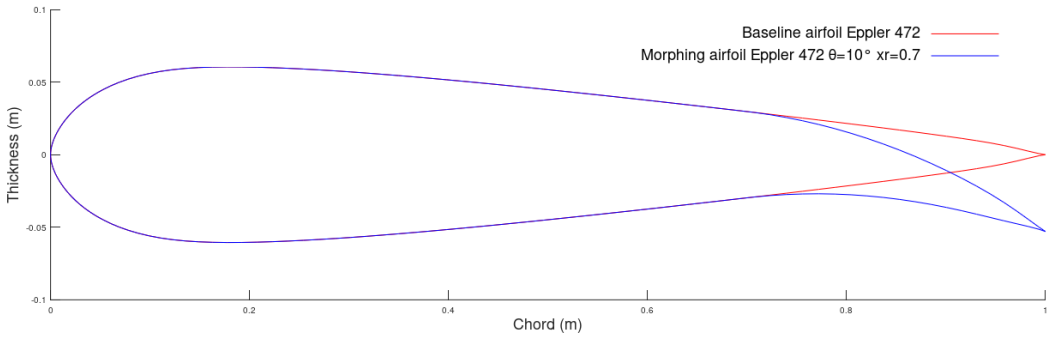

Figure 2. The profile of Eppler 472 in red baseline airfoil and in blue morphed with 70% rigid chord.

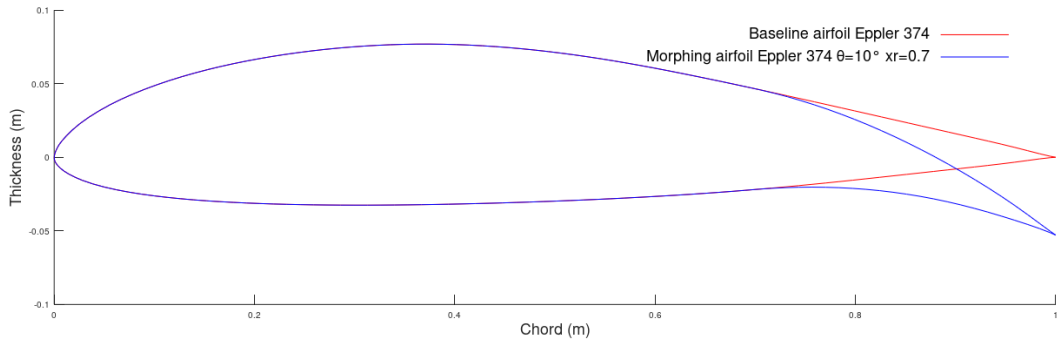

Figure 3. The profile of Eppler 374 in red baseline airfoil and in blue morphed with 70% rigid chord.

Figure 2 and Figure 3 shows in red the baseline airfoil and in blue the morphed airfoil with 70% of rigid chord, as can be seen, this is the portion of leading edge fixed. The morphed profiles were generated by MATLAB using the same equation of Woods & Friswell (2012) whereupon the camber line was assumed to deflect according to:

$$y_{spine} = \begin{cases} 0, & 0 \le x \le x_r \\ k \cdot (x - x_r)^2, & x_r < x \le 1 \end{cases} \quad (1)$$

where y_{spine} is the normalized y-coordinate of the neutral axis of the bending spine, x is the non-dimensional chord, k is the deflection coefficient, and x_r is the end of the rigid leading edge. This shape function was chosen because it is equivalent to the shape on a Euler Bernoulli beam of constant cross section under a concentrated tip moment. While not equivalent to the actual structure and loading of the FishBAC mechanism, it is representative (Woods & Friswell, 2012).

In order to quantify the deflection of the camber line at the trailing edge, an angle 'θ' was introduced. It is related geometrically with parameter k, resulting in a more accurate comparison of aerodynamic results when compared to the flap geometry. This angle is formed between the straight line connecting the start of morphing to the trailing edge of the morphed airfoil and the camber line of the baseline airfoil. In this study, the morphing angles used are in a range from 5° to 15°.

2.2 XFLR5 Analysis

The XFRL5 panel method was used as a primary study to estimate the aerodynamic performance of the 2D geometries generated by FishBAC concept and compare the results with the same airfoil using trailing-edge plain flaps. The algorithm is based on the XFOIL code which was developed to rapidly predict airfoil performance and its convergence is achieved by the interaction between the outer and inner flow solutions on the boundary layer displacement thickness. (XFRL5 Guidelines, 2013)

The XFRL5 code applies a high-order panel method which uses a linear-vorticity stream function to solve the flow field, producing streamlines along the boundaries of the airfoil which prevent the flow passing through the boundaries of the airfoil. An inviscid flow is assumed by the linear-vorticity theory which affects the analysis of the viscous drag effects. To improve the prediction of drag the XFRL5 incorporated a viscous formulation to calculate skin friction and flow separation. (Huntley, Allen, & Woods, 2019)

The XFRL5 code also includes a transition model to predict the transition from laminar to turbulent and is modeled over the airfoil based on the given co-ordinates. Furthermore, it is necessary other inputs, as the aerodynamic conditions of interest, the Reynolds and the Mach numbers and the angles of analysis.

2.3 CFD Analysis

There are some limitations when applying XFOIL panel method. Therefore, a well-established high-fidelity Computational Fluid Dynamics (CFD) solver is also used to investigate the aerodynamic performance of camber morphing airfoils. (Huntley, Allen, & Woods, 2019)

The analysis was done by software ANSYS - FLUENT to access higher accuracy in the results that were previously obtained by the XFLR5. The Computational Fluid Dynamics (CFD) analysis consists of solving major energy and transport equations applied to a pre-defined domain.

When considering a low- Reynolds - number flow, as presented in this study, a recently transitional model was introduced as shear-stress transport (SST) $\gamma - Re_\theta$ model or SST Transition model, that couple the SST model with transport equations for the intermittency and momentum-thickness Reynolds number (ANSYS, 2013). Four transport equations are solved, the first two are similar to the traditional K-ω model which incorporates the effects of Low-Reynolds numbers, compressibility and shear flow spreading based on the turbulence kinetic energy (k) and the specific dissipation rate (ω). The two additional transport equations are based on intermittency (γ) and the transitional onset Reynolds no. (Re_θ) that is the critical Reynolds number where intermittency starts (Meter, et al., 2006). The equations are given as follows:

$$\frac{\partial}{\partial t}(\rho k) + \frac{\partial}{\partial x_i}(\rho k u_i) = \frac{\partial}{\partial x_j}\left(\Gamma_k \frac{\partial k}{\partial x_j}\right) + G_k - Y_k + S_k \quad (2)$$

$$\frac{\partial}{\partial t}(\rho \omega) + \frac{\partial}{\partial x_i}(\rho \omega u_i) = \frac{\partial}{\partial x_j}\left(\Gamma_\omega \frac{\partial \omega}{\partial x_j}\right) + G_\omega - Y_\omega + S_\omega \quad (3)$$

$$\frac{\partial}{\partial t}(\rho \gamma) + \frac{\partial}{\partial x_j}(\rho \gamma U_j) = P_{\gamma 1} - E_{y1} + P_{y2} - E_{y2} + \frac{\partial}{\partial x_j}\left(\left(\mu + \frac{\mu_t}{\sigma_\gamma}\right)\frac{\partial \gamma}{\partial x_j}\right) \quad (4)$$

$$\frac{\partial}{\partial t}(\rho Re_\theta) + \frac{\partial}{\partial x_j}(\rho U_j Re_\theta) = P_{\theta t} + \frac{\partial}{\partial x_j}\left[\sigma_{\theta t}(\mu + \mu_t)\frac{\partial \widetilde{Re}_{\theta t}}{\partial x_j}\right] \quad (5)$$

The coupling of transitional model with SST K-ω is performed by ANSYS modifying the K-equation.

$$\frac{\partial}{\partial t}(\rho k) + \frac{\partial}{\partial x_i}(\rho k u_i) = \frac{\partial}{\partial x_j}\left(\Gamma_k \frac{\partial k}{\partial x_j}\right) + G_k^* - Y_k^* + S_k \tag{6}$$

$$G_k^* = \gamma_{eff} \bar{G}_k \tag{7}$$

$$Y_k^* = min\,(max\,(\gamma_{eff}, 0.1), 1.0) Y_k \tag{8}$$

2.4 Mesh generation

The high fidelity is related to a good discretization, which is achieved by applying a mesh in the geometry. There are many techniques applied to the process of generating the mesh with good quality, two of them that were applied in the current study are the inflation, which is used to capture the boundary layer effects creating thin prismatic elements adjacent to the geometry wall, and the bias factor, allowing exponential growth in the size of elements in the same edge.

A C- type structured mesh was used for both baseline and morphed configurations. The C segment measures 10 chords (10 meter) and the rectangular block measures 20c x 20c. The Figure 4 shows the generated mesh that was used for both baseline and morphed configurations, in the upper left the entire domain, upper right the detailed inflation zone around airfoil leading edge and lower right and left the morphed Eppler 472 and Eppler 374 airfoil respectively.

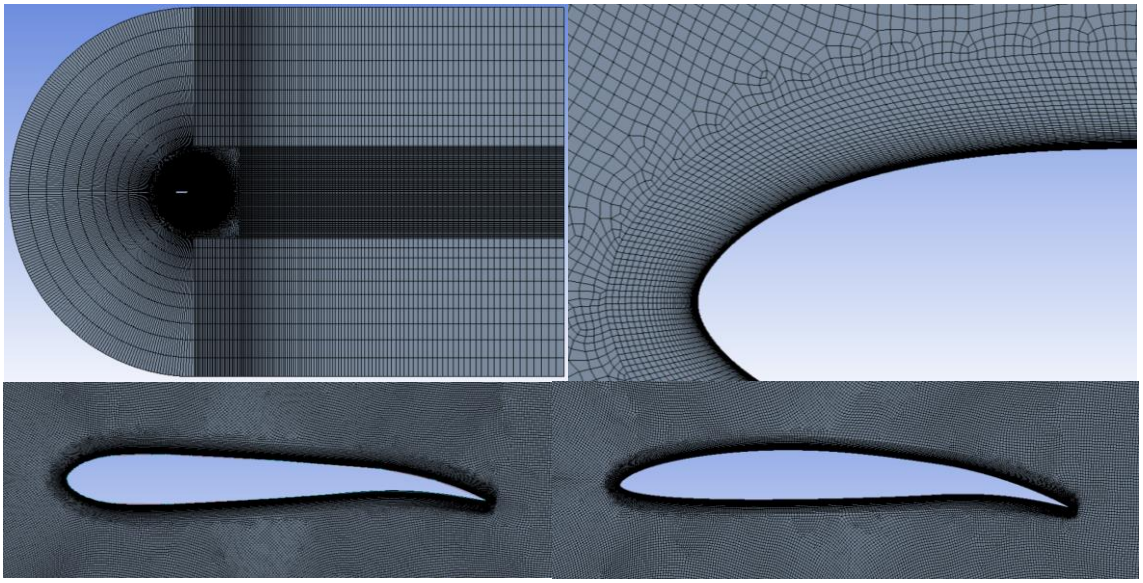

Figure 4. C-type mesh (upper left), inflation (upper right), mesh near Eppler 472 airfoil (lower left) and mesh near Eppler 374 airfoil (lower right)

The parameter Y^+ is defined as the non-dimensional wall distance for wall-bonded flow in a turbulence boundary layer analysis, which is related to the fully capitation of the physical phenomena in this region. In order to obtain reliable results, the distance of first layer thickness must be less than Y^+=1. Hence, for Eppler 374 simulation a first layer thickness of 0.04 mm with 45 layers is used and for Eppler 472 a first layer thickness of 0.07 mm with 48 layers is applied seeking Y^+=1 for each Reynolds number.

2.5 Boundary conditions

Two different sets of boundary conditions were used for zero and positive angles of attack. The first set for $\alpha = 0°$ the C portion of the boundary was set to velocity inlet; the upper and lower boundaries of the rectangle were set to a symmetry condition and the right boundary of the rectangle was made pressure outlet. The second set for cases with $\alpha > 0°$ a velocity inlet boundary condition was imposed on the C portion and lower boundary of the rectangle while the right and upper

was established as pressure outlet. The boundaries conditions for zero and positives angles of attack are shown in Figure 5.

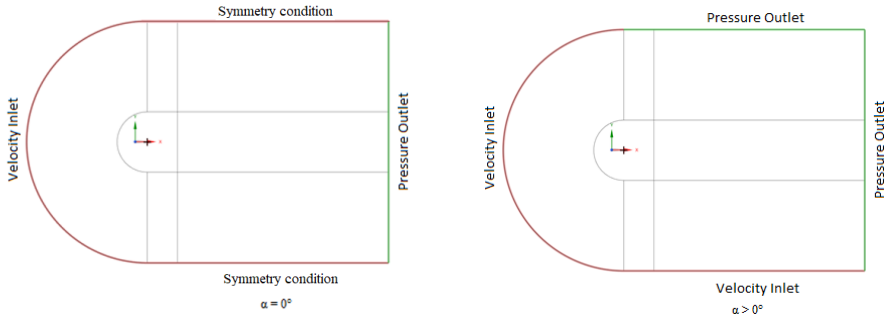

Figure 5. Boundaries conditions for α = 0° (left) and boundaries conditions for cases with α > 0° (right).

2.6 Mesh convergence study

As mentioned before, a good discretization of the domain is important to achieve high fidelity results. Therefore, a mesh convergence study was performed, to better understand the impacts of the different techniques used to create the mesh. The study consists of a series of CFD simulations with the same conditions and parameters, only varying the number of elements present in the mesh, which can be controlled by using different techniques of refinement.

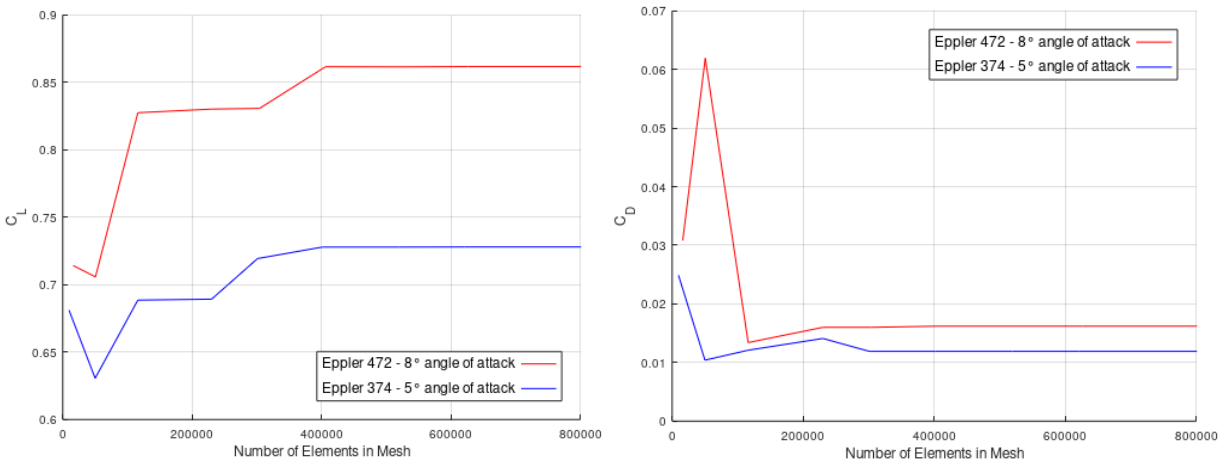

Figure 6. Lift coefficient curve (left) and drag coefficient curve (right) against number of elements in mesh.

The CFD simulations using Fluent were done at 8° angle of attack for Eppler 472 and at 5° angle of attack for Eppler 374, and the lift coefficient and drag coefficient against the number of elements in mesh are plotted in Figure 6. As can be seen from the figure, both lift and drag coefficients values remain unchanged, independent from the number of elements present in the mesh, at around four hundred thousand elements, is undoubtedly to say that any higher number of elements would only impact the time processing of the following analysis without much benefit. Thus, four hundred thousand elements were chosen for the following CFD simulations of this study.

2.7 Turbulence model validation

Before performing analyses of camber morphing airfoils, it is important to validate the turbulence solver against experimental data. Thus, both baseline Eppler 472 and Eppler 374 airfoils were chosen for this study as they are the only airfoils used in the following sections. The experimental results for the Eppler 472 are taken from the study of (Selig, Lyon, Broeren, Giguère, & Gopalarathnam, 1997) and for the Eppler 374 are taken from (Selig, Lyon, Giguere, Ninham, & Guglielmo, 1996), which both have a robust experimental data set available of low Reynolds number.

As can be seen in Figure 7, the experimental data for Eppler 472 and Eppler 374 airfoils, both with chord length 1 meter, were computed with a 0.5 x 10^6 and 0.3 x 10^6 Reynolds number respectively, are in good agreement with the numerical results obtained with the SST Transition turbulence model for the same Reynolds numbers. By looking at the lift polar curves very similar, wherein, they have the same values of stall angle and maximum lift coefficient.

Moreover, due to the fact the most common turbulence models cannot calculate the transition point from laminar to turbulent, this turbulence model was chosen because it solves these specific transition regions and does not overpredict the drag coefficient. Therefore, it can be said that the numerical results presented in this work are reliable and well represent the physical phenomenon.

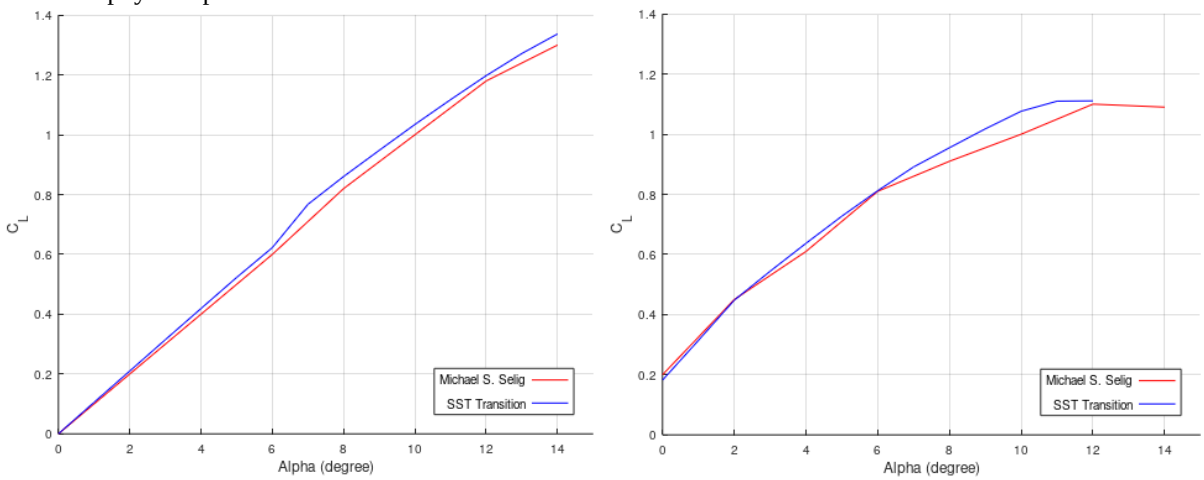

Figure 7. Comparison between experimental data from Michael S. Selig and SST Transition turbulence model simulation result of the lift coefficient curve for Eppler 472 airfoil (left) and for Eppler 374 airfoil (right).

3. RESULTS

In this section, based on the methodology, the comparison of aerodynamic characteristics obtained from XFLR5 and ANSYS-FLUENT simulations will be presented and discussed. Moreover, it was possible to choose the best morphed and flap geometries for the two airfoils, wherein, it was looked for CL x Alpha curves which were equal or very close for a given morphed and flap configuration, making the lift coefficient value equal at the same angle of attack to perform the analyses. Thus, the drag coefficient value and aerodynamic efficiency were verified depending on the geometric approach.

To further compare, an initial study was performed using a fast but low-fidelity tool (XFLR5), due to the large number of possible geometry cases to be analyzed. The flow simulations for various angles of attack and different configurations for flap and morphing concept were done for both Eppler 472 and Eppler 374 airfoils with a 0.5 x 10^6 and 0.3 x 10^6 Reynolds number respectively.

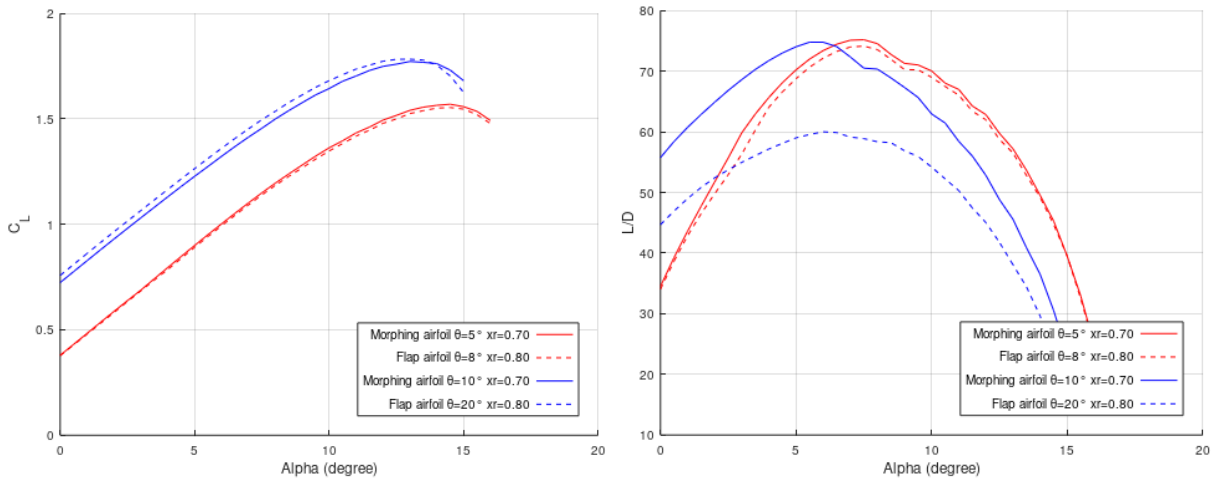

Figure 8. Lift polar (left) and Lift-to-drag ratio (right) for Eppler 472 airfoil.

In Figure 8 for the Eppler 472 airfoil the lift polar, as expected, shows that the predictions for the lift coefficient, C_L, versus angle of attack for both configurations, morphing and flap, are in close agreement for most angles of attack. Moreover, when increased the deflection from 5 to 10 degrees, for the morphing, and 8 to 20 degrees, for the flap, the C_L results obtained are higher, but the stall is predicted earlier. The lift-to-drag ratio, L/D, versus angle of attack shows significant improvements in aerodynamic efficiency obtained with the morphing over flapped configuration, for the first configuration with a deflection of 5 degrees, for the morphing, and 8 degrees, for the flap, there is an 1.4% increase in

maximum L/D and for the second configuration of 10 and 20 degrees the increase obtained is 25% for the maximum L/D. This behavior shows that with higher deflections the morphing is able to provide better improvements in aerodynamic efficiency.

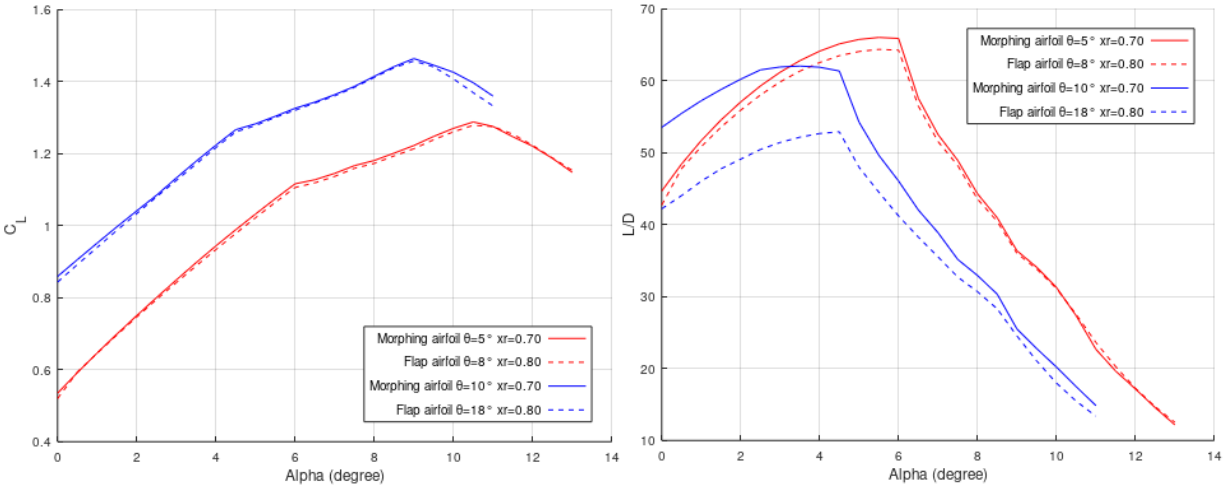

Figure 9. Lift polar (left) and Lift-to-drag ratio (right) for Eppler 374 airfoil.

In the same way, as was observed in the lift polar for Eppler 472, Figure 9 presents the predictions for the lift coefficient, C_L, versus angle of attack for both configurations morphing and flap for the Eppler 374 airfoil and the curves are in agreement for most of the angles of attack. As the behavior of the Eppler 472, when increased the deflection from 5 to 10 degrees, for the morphing, and 8 to 18 degrees, for the flap, the C_L results obtained are higher, but the stall is predicted earlier. The lift-to-drag ratio, L/D, versus angle of attack shows significant improvements in aerodynamic efficiency obtained with the morphing over flapped configuration, for the first configuration with a deflection of 5 degrees, for the morphing, and 8 degrees, for the flap, there is an 2.5% increase in maximum L/D and for the second configuration of 10 and 18 degrees the increase obtained is an 28%. This behavior shows that with higher deflections the morphing can provide better improvements in aerodynamic efficiency.

In this study so far, results for aerodynamic performance with laminar flow have been obtained, with transition points from laminar to turbulent flow being used at the leading edge of the airfoil in XFLR5, therefore, a high-fidelity tool (ANSYS-FLUENT) will be used in order to get more accurate results. Using a Computational Fluid Dynamics (CFD) solver with the SST Transition turbulence model, the transition regions will be solved because even with low Reynolds number values used, regions with transition from laminar to turbulent flow can occur.

The CFD simulations from 0° to 20° angles of attack were done for both Eppler 472 and Eppler 374 airfoils with a 0.5 x 10^6 and 0.3 x 10^6 Reynolds number respectively. For these laminar and 2D simulations, the air density used was 1.225 kg/m³ and the dynamic viscosity of the air used was 1.789 x 10^{-5} Pa.s, resulting in a far-field velocity of 7.31 m/s for a 1-meter chord to Eppler 472 and 4.40 m/s to Eppler 374 using the same chord length. In addition to this, the flow will be assumed to be incompressible and permanent. Thus, the same flap and morphed geometries analyzed with the XFLR5, will be now simulated by CFD code and the results will be presented.

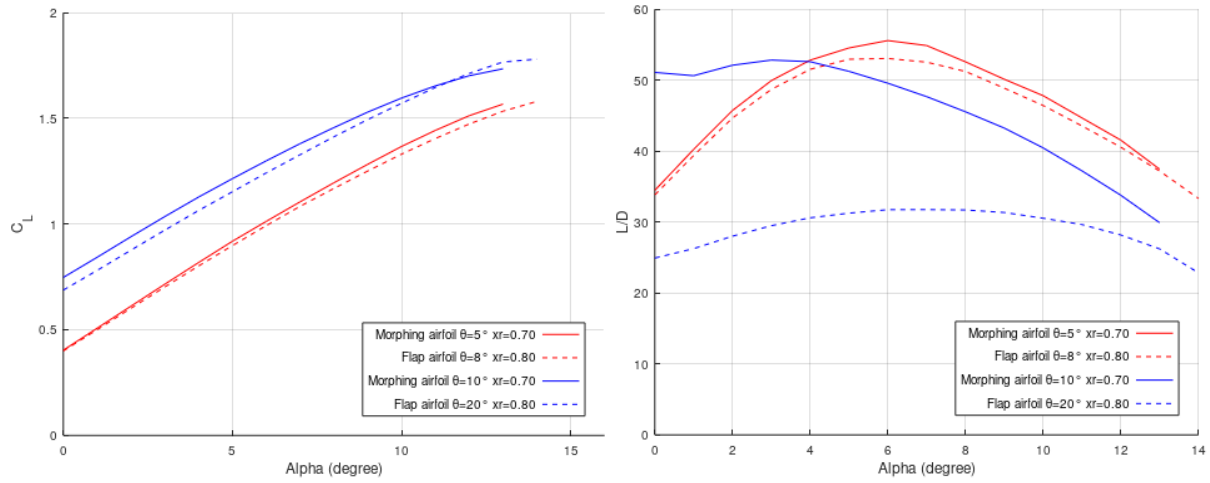

Figure 10. Lift polar (left) and Lift-to-drag ratio (right) for Eppler 472 airfoil.

Figure 10 shows the lift coefficient versus angle of attack and the aerodynamic performance (L/D) versus angle of attack for Eppler 472 as predicted by FLUENT. Similar to the XFLR5 comparison, the lift polar curve for the morph and flap configurations with little deflection are very close, with a maximum C_L close to 1.58 and a stall angle around 13°. On the other hand, the lift polar curve for both configurations with a higher deflection are not very similar on the beginning of the lines, but they have a certain agreement on the maximum lift coefficient value of 1.75 and a stall angle close to 13°. As can be seen, the lift-to-drag ratio versus angle of attack curve shows significant improvements in aerodynamic efficiency obtained with the morphing over flapped configuration, especially for higher deflections. For the first analysis with a deflection of 5 degrees, for the morphing, and 8 degrees, for the flap, there is an 5.0% increase in the L/D at angle of attack of 6° and for the second analysis of 10 and 20 degrees, for the morphed and flap configuration respectively, the increase obtained is 72% at angle of attack of 4°. These numerical results from CFD, similar to the results obtained using XFRL5, shows that with higher deflections the morphing can improve much more lift-to-drag ratio and with low deflections the results are very equal, showing a low drag penalty provided by symmetrical morphed geometries.

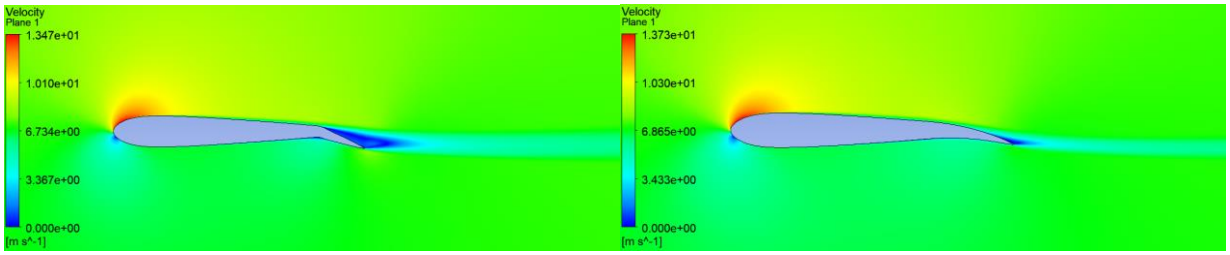

Figure 11. Velocity field at 4° angle of attack with the SST Transition turbulence model for the Eppler 472 with a 20° flap deflection (left) and for the morphed Eppler 472 with 10° of deflection (right).

In the Figure 11, it is possible to see the velocity field at 4° angle of attack with the SST Transition turbulence model for the Eppler 472 with a 20° flap deflection and for the morphed Eppler 472 with 10° of deflection, where the velocity increases on the upper surface and decreases on the lower surface of the airfoil. This speed difference also causes a pressure difference between the upper and lower surface, generating the lift force in the airfoil. In addition to this, it is possible to verify that there is a large region with detachment of the boundary layer, generating a strong drag force in the flap geometry. However, this low pressure region almost does not exist for morphed Eppler 472 geometry, proving the low drag penalty.

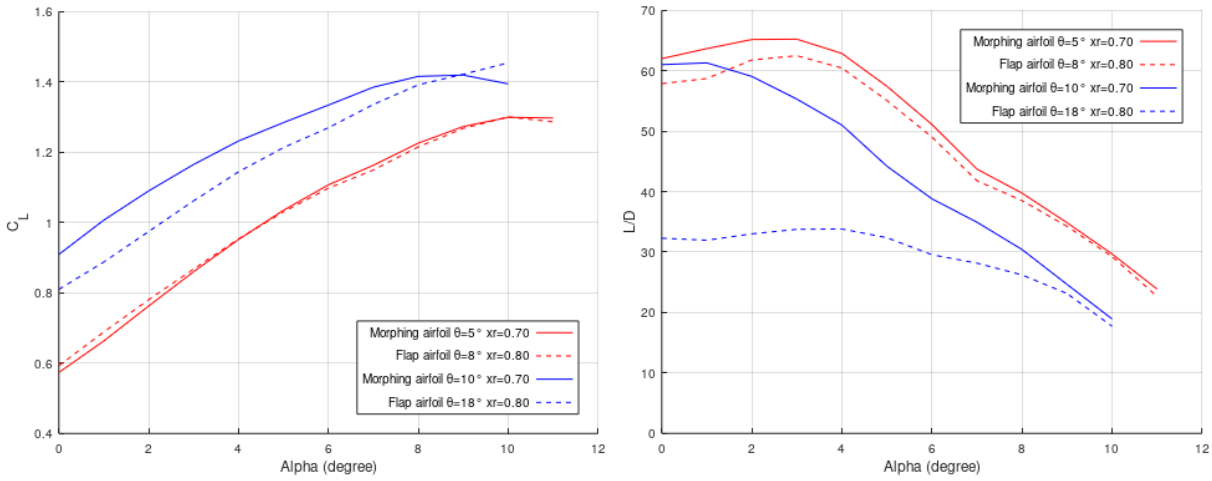

Figure 12. Lift polar (left) and Lift-to-drag ratio (right) for Eppler 374 airfoil.

The lift coefficient versus angle of attack and the aerodynamic performance (L/D) versus angle of attack for Eppler 374 in the Figure 12 were obtained from Fluent simulations. Similar to the XFLR5 comparison as well, the lift polar curve for the morph and flap configurations with little deflection are very equal, with a maximum C_L close to 1.29 and a stall angle around 10°. On the other hand, the lift polar curve for both configurations with a higher deflection are not very similar, but they have a certain agreement on the lift coefficient value of 1.42 at angle of attack of 9°, which is the stall angle for morphed geometry and almost for the flap configuration. It is possible to note that the main reason behind this difference are the lift coefficient results obtained for the 18° flap deflection configuration.

As can be seen in the Figure 12, the lift-to-drag ratio versus angle of attack curve shows significant improvements in aerodynamic efficiency obtained with the morphing over flapped configuration, especially for higher deflections. For the first analysis with a deflection of 5 degrees, for the morphing, and 8 degrees, for the flap, there is an 5.5% increase in the L/D at angle of attack of 2° and for the second analysis of 10 and 18 degrees, for the morphed and flap configuration respectively, the increase obtained is 79% at angle of attack of 2°. These numerical results from CFD shows that with higher deflections the morphing can improve much more lift-to-drag ratio and with low deflections the results are very equal, showing a low drag penalty provided by asymmetrical morphed geometries.

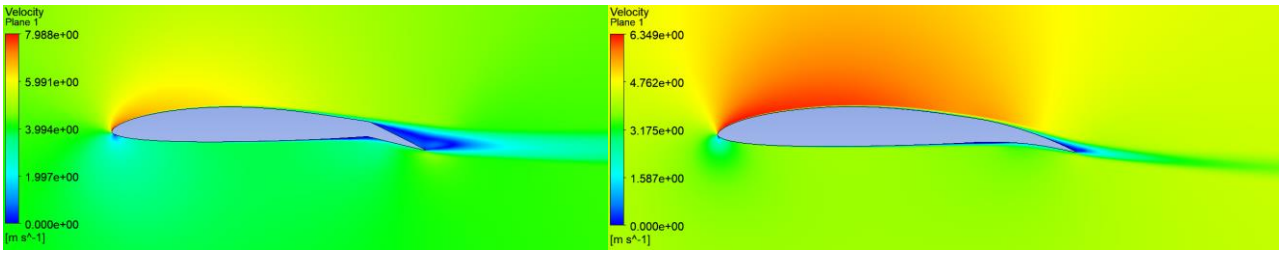

Figure 13. Velocity field at 4° angle of attack with the SST Transition turbulence model for the Eppler 374 with a 18° flap deflection (left) and for the morphed Eppler 374 with 10° of deflection (right).

From the Figure 13, it is possible to see the velocity field at 4° angle of attack with the SST Transition turbulence model for the Eppler 374 with a 18° flap deflection and for the morphed Eppler 374 with 10° of deflection, where the velocity also increases on the upper surface and decreases on the lower surface of the airfoil. This difference causes a pressure difference between the upper and lower surface, which is amplified due to the curvature present in the asymmetric airfoil, generating a strong lift force in the airfoil at low angles of attack. In addition to this, it is also possible to verify that there is a large region with boundary layer separation on the flap geometry, generating a strong drag force. However, this separation region is barely present in the morphed Eppler 374 geometry, proving the low drag penalty as well.

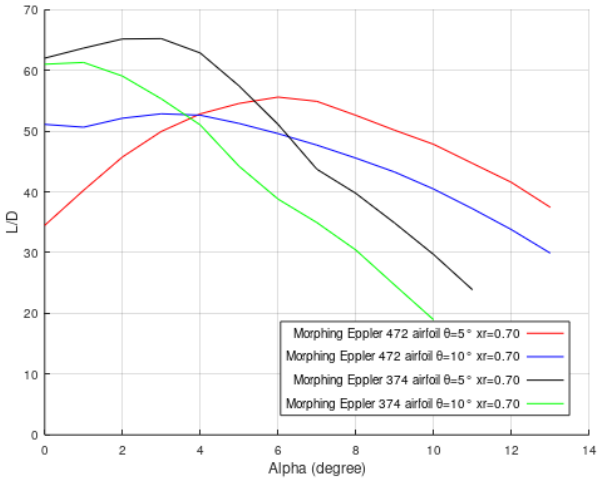

Figure 14. Aerodynamic efficiency for all Eppler 472 and Eppler 374 morphing configurations.

After performing all the CFD simulations, as can be seen from Figure 14, the morphed asymmetric Eppler 374 with a 5° of deflection has the greatest aerodynamic efficiency for angles of attack between 0° to 5°. Proving the advantage of the curvature already present in the airfoil plus the morphing concept and it is also possible to note that the rigid part of the leading edge was fixed at 70% as this region is commonly used as fuel tank in a real application wing.

4. CONCLUSIONS

This work has investigated the aerodynamics characteristics of camber morphing airfoils against geometries with plain flap mechanism, inwhich low Reynolds numbers were fixed and the angle of attack was varied for the Eppler 472 and for the Eppler 374, in order to verify which airfoil and its configuration (morphed or with a flap) would be more efficient aerodynamically. The aerodynamic coefficients are estimated using a CFD solver (Fluent) and XFoil (XFLR5). The following points are observed from this study:

1) Both Fluent and XFLR5 predict nearly similar results as they employ a transition model. Where SST Transition turbulence model used in Fluent was validated and provided close results in comparison with the experimental data, thus, it can be stated that the numerical results presented in this work are reliable and well represent the physical phenomenon.
2) The reduction in the drag coefficient in the morphed geometries is noticeable, leading to a better lift-to-drag ratio curve when compared to the plain flap configurations and this behavior occurs for both Fluent and XFLR5. It is also possible to affirm that small to moderate camber morphing deflections provide significant increases in lift coefficient with small increases in drag coefficient, confirming the low drag penalty.
3) The smooth and continuous changes in geometry provided by the concept of camber morphing can significantly improve the lift-drag ratio when compared to plain flaps, due to the deformation characteristic that can delay the separation of the boundary layer, thus reducing the drag force caused by this low-pressure region. Moreover, when applying morphing configuration to an extension larger than 30%, the results are even more significant.
4) The symmetrical or asymmetrical characteristic of the airfoils has a large influence on the aerodynamic coefficients, especially when the morphing concept is used, due to the drag reduction. The main advantage of asymmetrical characteristic is the gains in lift force when compared with symmetrical geometries, as well-known.

5. ACKNOWLEDGEMENTS

The authors gratefully acknowledge IMT-Maua Institute of Technology for supporting their research activities.

6. REFERENCES

ANSYS, G. (2013). *ANSYS Fluent Theory Guide.* ANSYS, Inc, Canonsburg.

Barbarino, S., Bilgen, O., Ajaj, R. M., Friswell, M. I., & Inman, D. J. (Junho de 2011). A Review of Morphing Aircraft. *Journal of Intelligent Material Systems and Structures, 22*(9), 823 - 877.

Huntley, S. J., Allen, C. B., & Woods, B. K. (2019). *Computational Analysis of the Aerodynamics of Camber Morphing.* Dallas.

Meter, F. R., Langtry, R. B., Likki, S. R., Suzen, Y. B., Huang, P. G., & Völker, S. (2006). A Correlation-Based Transition Model Using Local Variables—Part I: Model Formulation. *Jornal of Turbomachinery*.

Selig, M., Lyon, C., Broeren, A., Giguère, P., & Gopalarathnam, A. (1997). *Summary of Low-Speed Airfoil Data* (Vol. 3). Virginia Beach: SoarTech Publications.

Selig, M., Lyon, C., Giguere, P., Ninham, C., & Guglielmo, J. (1996). *Summary of Low-Speed Airfoil Data* (Vol. 2). Virginia Beach: SoarTech Publications.

Woods, B. K., & Friswell, M. I. (2012). Preliminary Investigation of a Fishbone Active Camber Concept. *ASME 2012 Conference on Smart Materials, Adaptive Structures and Intelligent Systems* (pp. 1-9). Stone Montain: ASME.

XFRL5 Guidelines. (2013). *Analysis of foils and wings operating at low Reynolds numbers.*

7. RESPONSIBILITY NOTICE

The authors are the only responsible for the printed material included in this paper.